Tracking Sliding Clamp Opening and Closing during Bacteriophage T4 DNA Polymerase Holoenzyme Assembly †

ARTICLE *in* BIOCHEMISTRY · APRIL 2000

Impact Factor: 3.02 · DOI: 10.1021/bi992377r · Source: PubMed

Tracking Sliding Clamp Opening and Closing during Bacteriophage T4 DNA Polymerase Holoenzyme Assembly†

Stephen C. Alley, Ernesto Abel-Santos, and Stephen J. Benkovic*

Department of Chemistry, 414 Wartik Laboratory,The Pennsylvania State University, University Park, Pennsylvania 16802

Received October 13, 1999; Revised Manuscript Received December 22, 1999

ABSTRACT: The bacteriophage T4 DNA polymerase holoenzyme, consisting of the DNA polymerase (gp43), the sliding clamp (gp45), and the clamp loader (gp44/62), is loaded onto DNA in an ATP-dependent, multistep reaction. The trimeric, ring-shaped gp45 is loaded onto DNA such that the DNA passes through the center of the ring. gp43 binds to this complex, thereby forming a topological link with the DNA and increasing its processivity. Using stopped-flow fluorescence-resonance energy transfer, we have investigated opening and closing of the gp45 ring during the holoenzyme assembly process. Two amino acids that lie on opposite sides of the gp45 subunit interface, W91 and V162C labeled with coumarin, were used as the fluorescence donor and acceptor, respectively. Free in solution, gp45 has two closed subunit interfaces with W91 to V162-coumarin distances of 19 Å and one open subunit interface with a W91 to V162C-coumarin distance of 40 Å. Making the assumption that the distance across the two closed subunit interfaces is unchanged during the holoenzyme assembly process, we have found that the distance across the open subunit interface is first increased to greater than 45 Å and is then decreased to 30 Å during a 10-step assembly mechanism. The gp45 ring is not completely closed in the holoenzyme complex, consistent with previous evidence suggesting that the C-terminus of gp43 is inserted into the gp45 subunit interface. Unexpectedly, ATP-hydrolysis events are coupled to only a fraction of the total distance change, with conformational changes linked to binding DNA and gp43 coupled to the majority of the total distance change. Using the nonhydrolyzable ATP analogue ATP-γ-S results in formation of a nonproductive gp45•gp44/62 complex; however, adding an excess of ATP to this nonproductive complex results in rapid ATP/ATP-γ-S exchange to yield a productive gp45•gp44/62 complex within seconds.

DNA replication requires the coordinated action of several proteins to construct a replication complex or holoenzyme. In bacteriophage T4, the holoenzyme is composed of the DNA polymerase (gp43), the DNA polymerase processivity factor, or sliding clamp (gp45), and the clamp-loading protein (a 4:1 complex of gp44 and gp62). Analogues of these proteins are found in *Escherichia coli*, where DNA polymerase III, the β clamp, and the clamp-loading γ complex form the holoenzyme, as well as in eukaryotes, where DNA polymerase δ, the PCNA clamp, and the clamp-loading RF−C complex form the holoenzyme (*1*, *2*). X-ray crystallography has shown gp45 (J. Kuriyan, personal communication), the β clamp (*3*), and PCNA (*4*) to be multimeric, ring-shaped complexes, with the newly synthesized DNA presumably traveling through the centers of the rings. The β clamp is a dimer, while gp45 and PCNA are trimers, and in all three cases the individual subunits are arranged head-to-tail to form identical subunit interfaces. The clamp-loading proteins are all multisubunit ATPases, with ATP hydrolysis required to form the holoenzyme. gp44/62 is only a transient part of the bacteriophage T4 holoenzyme: following clamp loading, it chaperones gp43 to the gp45•DNA complex and then dissociates (*5*). The γ complex dissociates from the β clamp after loading but remains associated with the τ subunit, the bridge between the leading and lagging strand DNA polymerases in the holoenzyme (*6*, *7*). RF−C was likewise found to dissociate from PCNA after loading (*8*).

The X-ray crystal structure of gp43 from bacteriophage RB69 [63% identity with bacteriophage T4 (*9*)] has been solved (*10*). We recently showed that the C-terminal tail of gp43, which is absolutely required for holoenzyme assembly (*11*), interacts with amino acids at the subunit interface of gp45 and suggested that this tail is inserted into the subunit interface of gp45 (*12*). The location of the interaction between gp45 and gp44/62 is at present unknown, and as such a detailed three-dimensional picture of the bacteriophage T4 holoenzyme during assembly awaits elucidation.

The kinetic mechanisms of holoenzyme assembly in bacteriophage T4 (*13*, *15*) and *E. coli* (*16*-*18*) have been investigated by a variety of steady-state and pre-steady-state techniques. Both of these holoenzymes have been shown to be assembled in many steps proceeding through several discrete structural complexes. In bacteriophage T4, gp44/62 hydrolyzes two molecules of ATP upon interaction with gp45 and then two more molecules of ATP upon interaction with DNA (*15*, *19*, *20*), with a conformational change in the gp45•gp44/62•DNA complex coupled to ATP hydrolysis being the rate-limiting step in holoenzyme assembly (*15*, *19*). This

† This work was supported by National Institutes of Health Grants GM13306 (S.J.B.) and GM19492 (S.C.A.).

* To whom correspondence should be addressed: E-mail: sjb1@psu.edu. Phone: (814) 865-2882. Fax: (814) 865-2973.

10.1021/bi992377r CCC: $19.00
Published on Web 02/25/2000

results in a burst of ATP hydrolysis by gp44/62 being observable by rapid-quench techniques (*15*, *19*, *20*). In contrast, the *E. coli* γ complex hydrolyzes two to three molecules of ATP (*21*), with ATP hydrolysis following the assembly of a β clamp·γ complex·DNA complex (*18*). The exact nature of the ATP-hydrolysis events as well as that of the conformational changes required in loading the ring-shaped sliding clamps onto DNA in these two organisms have not been assigned.

In the present report, we have used fluorescence-resonance energy transfer (FRET)[1] and pre-steady-state kinetic techniques to investigate the conformational changes that gp45 undergoes as it is loaded onto DNA by gp44/62 and assembled into the holoenzyme with gp43. We have taken advantage of a tryptophan near the subunit interface (W91) as a fluorescence donor and placed the fluorescence acceptor coumarin on the opposite side of the subunit interface (V162C−CPM). With this system, the distance across the gp45 subunit interface can be monitored during holoenzyme assembly by stopped-flow FRET. We have previously shown that one of the three gp45 subunit interfaces is open in solution, with the distance between W91 and V162C−CPM of 35−38 Å, and the other two subunit interfaces are closed, with W91 to V162C−CPM distances of 19 Å (*22*). Making the assumption that the two closed subunit interfaces maintain their W91 to V162C−CPM distances during holoenzyme assembly, we have found in the present study that the open gp45 subunit interface undergoes seven conformational changes during a 10-step mechanism, with both opening and closing of this subunit interface observed. The final W91 to V162C−CPM distance of the open subunit interface is 30 Å, suggesting that gp45 is not completely closed in the holoenzyme. ATP hydrolysis by gp44/62 only powers a fraction of gp45 opening and closing, and it does not drive gp44/62 disassociation: ATP hydrolysis causes two openings of the gp45 subunit interface, the first at least 4 Å and the second 2 Å. Successive interactions of gp45 with DNA and gp43 cause gp45 ring closure, covering a total distance of at least 15 Å. We propose that ATP hydrolysis by gp44/62 is causing conformational changes in gp44/62 that prepare it for interaction with the next holoenzyme component (first with DNA and second with gp43) in order to optimize the catalytic efficiency of holoenzyme assembly.

EXPERIMENTAL PROCEDURES

Materials and Their Sources. DNA substrates were synthesized and purified as previously described (*22*). CPM was obtained from Molecular Probes (Eugene, OR). ATP and ATP-γ-S were from Boehringer-Mannheim (Indianapolis, IN). Deep $Vent_R$ DNA Polymerase and all restriction enzymes were from New England Biolabs (Beverly, MA). L-Tryptophan and streptavidin were from Sigma (St. Louis, MO). All other chemicals were of analytical grade or better.

Proteins and Labeling. The gp45 mutant V162C/W198F was purified and labeled with CPM as previously described (*22*). Wild-type gp45, gp44/62, and exonuclease-deficient gp43 were purified as described earlier (*23*−*25*). gp43Δ6 was purified as previously described (*11*). The W91F/V162C/W198F mutant was cloned using the following PCR primers: (A) 5′-GCG GAA TTC CAT ATG AAA CTG TCT AAA GAT, (B) 5′-GCG GAA TTC GGA TTC CTA TTA AAA ATC GTG GGT, (C) 5′-CGC TCA ACA ATT TTT TTC CCG GCC GCC GAT CCG AGT ACA, (D) 5′-TGT ACT CGG ATC GGC GGC CGG GAA AAA AAT TGT TGA GCG. The fragments AD and BC were prepared by PCR using pET26b-V162C/W198F (*22*) as a template. Overlap extension PCR yielded the mutant 45 gene W91F/V162C/W198F that included a new *Bsi*EI site. This full-length fragment was digested with *Nde*I and *Bam*HI and ligated into pET26b digested previously with *Nde*I and *Bam*HI to yield pET26b-W91F/V162C/W198F. Purification and labeling with CPM were as reported previously (*22*). Mutations were verified by DNA sequencing. The ability of the W91F/V162C/W198F mutant, in both unlabeled and CPM-labeled forms, to stimulate the ATPase activity of gp44/62 and enable strand-displacement DNA synthesis by gp43 was confirmed as described earlier (*22*). Protein concentrations were determined by a Bradford protein assay (BioRad, Hercules, CA).

Stopped-Flow FRET. Stopped-flow experiments were performed on an Applied Photophysics (Leatherhead, Surrey, U.K.) SX.18MV stopped-flow reaction analyzer in fluorescence mode at a constant temperature of 25 °C. The excitation wavelength was 290 or 390 nm, the slit width was 10 nm, and a 420 nm cutoff filter was placed in front of the emission photomultipier tube. By exciting at 290 nm and detecting all fluorescence above 420 nm, we were able to observe FRET between tryptophan and V162C−CPM as well as fluorescence from direct excitation of CPM without any contribution from tryptophan fluorescence. By exciting at 390 nm, we were able to observe exclusively fluorescence from direct CPM excitation. The excitation and emission path lengths were both 2 mm. Single or split timebases were used as appropriate, with 2000 total data points collected.

The W91 to V162C−CPM distances can be calculated using the following relationships for fluorescent acceptor sensitization (*26*):

$$E_T = \left(\frac{I_{AD}}{I_A} - 1\right)\left(\frac{\epsilon_A}{\epsilon_D}\right) \quad (1)$$

$$R = R_o \sqrt[6]{\frac{1}{E_T} - 1} \quad (2)$$

where E_T is the transfer efficiency of the FRET process, I_{AD} and I_A are the fluorescent intensities of the CPM acceptor in the presence and absence, respectively, of the tryptophan donor at the donor excitation wavelength (290 nm), ϵ_A and ϵ_D are the extinction coefficients of the CPM acceptor and tryptophan donor, respectively, at the donor excitation wavelength (290 nm), R_o is the Förster distance at which the transfer efficiency is 50%, and R is the distance between

[1] Abbreviations: bio, biotin; bp, base pairs; CPM, 7-diethylamino-3-(4′-maleimidylphenyl)-4-methylcoumarin; F_A^{290}, normalized change in fluorescence of the acceptor in the absence of the donor when excited at 290 nm; F_{AD}^{290}, normalized change in fluorescence of the acceptor in the presence of the donor when excited at 290 nm; F_A^{390}, normalized change in fluorescence of the acceptor in the absence of the donor when excited at 390 nm; FRET, fluorescence-resonance energy transfer; I_A, fluorescence intensity of the acceptor in the absence of the donor; I_{AD}, fluorescence intensity of the acceptor in the presence of the donor; Tris, tris(hydroxymethyl)aminomethane.

Table 1: Fluorescence Parameters and Transfer Efficiencies for gp45 versus gp44/62 and ATP, gp45, gp44/62, and ATP versus EDTA, and gp45 versus gp43

assembly state[a]	F_{AD}^{290} [b]	F_{A}^{290} [b]	F_{A}^{390} [b]	$I_{AD} + X$ [c,d]	$I_A + X$ [d,e]	I_A [f]	X [d]	I_{AD}	I_{AD}/I_A	E_T
A	1.000[g]	1.000[g]	1.000[g]	1.85[h]	1.00[h]	1.00[h]	0.00	1.85	1.85	0.692
B	1.000[i]	1.000[i]	1.000[i]	1.85	1.00	1.00	0.00	1.85	1.85	0.692
C	1.158 ± 0.013[j]	1.252 ± 0.011[j]	1.054 ± 0.006[j]	2.142 ± 0.024	1.252 ± 0.011	1.054 ± 0.006	0.198 ± 0.013	1.944 ± 0.027	1.844 ± 0.028	0.688 ± 0.010
D	0.999 ± 0.006	1.084 ± 0.002[j]	1.001 ± 0.005	1.848 ± 0.011	1.084 ± 0.002	1.001 ± 0.005	0.083 ± 0.005	1.765 ± 0.012	1.763 ± 0.015	0.622 ± 0.005
L[k]	1.152 ± 0.001	1.169 ± 0.009	1.031 ± 0.001	2.131 ± 0.002	1.169 ± 0.009	1.031 ± 0.001	0.138 ± 0.009	1.993 ± 0.009	1.933 ± 0.009	0.760 ± 0.004
gp45·gp43[l]	1.263 ± 0.016[j]	1.308 ± 0.030[j]	1.041 ± 0.011[j]	2.337 ± 0.030	1.308 ± 0.030	1.041 ± 0.011	0.267 ± 0.032	2.070 ± 0.044	1.989 ± 0.047	0.806 ± 0.019

[a] States are shown in Scheme 1. [b] Normalized fluorescence values starting from $gp45^A$ equal to 1.0, where the superscript indicates the excitation wavelength and the subscript indicates which mutant was used in the measurement [V162C/W198F−CPM (AD) or W91F/V162C/W198F−CPM (A)]. [c] Determined by multiplying F_{AD}^{290} by the starting $I_{AD} + X$ value (assumed equal to 1.85, as determined in the steady state). [d] X is the amount of interprotein FRET (from gp44/62 and/or gp43 tryptophans to CPM on gp45). [e] Determined by multiplying F_{A}^{290} by the starting $I_A + X$ value (assumed equal to 1.00, as determined in the steady state). [f] Determined by multiplying F_{A}^{390} by the starting I_A value (assumed equal to 1.00, as determined in the steady state). [g] Starting state assumed equal to 1.0. [h] Determined from steady-state measurements. [i] No changes were observed from the previous state. [j] F_{max} as determined from eq 5 for saturating gp44/62 or gp43. [k] Determined from gp45, gp44/62, and ATP versus EDTA. [l] Determined from gp45 versus gp43.

Table 2: Fluorescence Parameters and Transfer Efficiencies for gp45, gp44/62, and ATP versus DNA and gp45, gp44/62, ATP, and DNA versus EDTA

assembly state[a]	F_{AD}^{290} [b]	F_{A}^{290} [b]	F_{A}^{390} [b]	$I_{AD} + X$ [c,d]	$I_A + X$ [d,e]	I_A [f]	X [d]	I_{AD}	I_{AD}/I_A	E_T
D	1.000[g]	1.000[g]	1.000[g]	1.848 ± 0.011	1.084 ± 0.002	1.001 ± 0.005	0.083 ± 0.005	1.765 ± 0.012	1.763 ± 0.015	0.622 ± 0.005
E	1.000[h]	1.000[h]	1.000[h]	1.848 ± 0.011	1.084 ± 0.002	1.001 ± 0.005	0.083 ± 0.005	1.765 ± 0.012	1.763 ± 0.015	0.622 ± 0.005
F	1.130 ± 0.013	1.051 ± 0.017	1.043 ± 0.011	2.088 ± 0.027	1.139 ± 0.018	1.044 ± 0.012	0.095 ± 0.022	1.993 ± 0.035	1.909 ± 0.040	0.741 ± 0.016
G	1.200 ± 0.005	1.137 ± 0.007	1.047 ± 0.007	2.218 ± 0.016	1.232 ± 0.008	1.048 ± 0.009	0.184 ± 0.012	2.034 ± 0.020	1.941 ± 0.025	0.767 ± 0.010
H	1.180 ± 0.005	1.128 ± 0.005	1.047 ± 0.007[h]	2.181 ± 0.016	1.223 ± 0.006	1.048 ± 0.009	0.175 ± 0.011	2.006 ± 0.019	1.914 ± 0.025	0.745 ± 0.010
M[i]	1.172 ± 0.006	1.094 ± 0.002	1.047 ± 0.007[h]	2.166 ± 0.017	1.186 ± 0.003	1.048 ± 0.009	0.138 ± 0.010	2.028 ± 0.020	1.935 ± 0.025	0.762 ± 0.010

[a] States are shown in Scheme 1. [b] Normalized fluorescence values starting from $gp45^D$ equal to 1.0, where the superscript indicates the excitation wavelength and the subscript indicates which mutant was used in the measurement [V162C/W198F−CPM (AD) or W91F/V162C/W198F−CPM (A)]. [c] Determined by multiplying F_{AD}^{290} by the starting $I_{AD} + X$ value (1.848 ± 0.011, as determined for state D from Table 1). [d] X is the amount of interprotein FRET (from gp44/62 and/or gp43 tryptophans to CPM on gp45). [e] Determined by multiplying F_{A}^{290} by the starting $I_A + X$ value (1.084 ± 0.002, as determined for state D from Table 1). [f] Determined by multiplying F_{A}^{390} by the starting I_A value (1.001 ± 0.005, as determined for state D from Table 1). [g] Starting state assumed equal to 1.0. [h] No changes were observed from the previous state. [i] Determined from gp45, gp44/62, ATP, and DNA versus EDTA.

the donor and acceptor. Changes in the I_{AD} term report changes in the intensity of the FRET (due to changes in the donor to acceptor distances) and changes in the intensity of the direct excitation of the CPM fluorophore (due to changes in the CPM environment), while changes in the I_A term report only changes in direct CPM excitation. R_o was previously determined to be 31 Å (*22*, *27*) as follows:

$$R_o = (0.211\phi_D\kappa^2\eta J)^{1/6} \quad (3)$$

where ϕ_D is the quantum yield of the donor (tryptophan), κ^2 is the orientation factor (determined from anisotropy measurements), η is the refractive index of the medium, and J is the overlap integral between the fluorescence spectrum of the donor and the absorption spectrum of the acceptor. We have assumed that the ϕ_D, κ^2, and J (and, therefore, R_o) values measured for V162C/W198F−CPM in complex buffer (*22*) are appropriate for the intermediate states of gp45 during holoenzyme assembly. Our previous assumption of κ^2 equal to $^2/_3$ (*22*) will result in errors in the R values reported in Table 4 to be less than 10% (*28*).

The I_{AD}/I_A ratio for gp45 in complex buffer was determined by steady-state fluorescence using an ISA (Edison, NJ) FluoroMax-2 spectrofluorimeter. V162C/W198F−CPM (I_{AD}) and W91/V162C/W198F−CPM (I_A) were independently placed in complex buffer and their fluorescence intensities measured at 476 nm upon excitation at 290 nm (2 nm slit width, 0.5 s integration time, and 2 mm excitation path length) to yield I_{AD}/I_A equal to 1.85.

The ϵ_A and ϵ_D values were measured at 290 nm using CPM and L-tryptophan, respectively, as model compounds, yielding $\epsilon_A = 3340\ M^{-1}\ cm^{-1}$ and $\epsilon_D = 4100\ M^{-1}\ cm^{-1}$. The transfer efficiency of gp45 in complex buffer was therefore determined to be 0.692 for CPM sensitization, consistent with the value of 0.75 found previously by tryptophan quenching (*22*).

Stopped-flow fluorescence experiments were conducted as follows: syringe A, containing the fluorophore and other components as indicated in the text and figure legends, was initially mixed with syringe B, containing only complex buffer (150 mM potassium acetate, 20 mM Tris, pH 7.5,

Table 3: Fluorescence Parameters and Transfer Efficiencies for gp45, gp44/62, ATP, and DNA versus gp43 and gp45, gp44/62, ATP, DNA, and gp43 versus EDTA

assembly state[a]	F_{AD}^{290} [b]	F_{A}^{290} [b]	F_{A}^{390} [b]	$I_{AD} + X$ [c,d]	$I_A + X$ [d,e]	I_A [f]	X[d]	I_{AD}	I_{AD}/I_A	E_T
H	1.000[g]	1.000[g]	1.000[g]	2.181 ± 0.016	1.223 ± 0.006	1.048 ± 0.009	0.175 ± 0.011	2.006 ± 0.019	1.914 ± 0.025	0.745 ± 0.010
I	1.000[h]	1.000[h]	1.000[h]	2.181 ± 0.016	1.223 ± 0.006	1.048 ± 0.009	0.175 ± 0.011	2.006 ± 0.019	1.914 ± 0.025	0.745 ± 0.010
J	1.083 ± 0.006	1.069 ± 0.005	1.025 ± 0.006	2.362 ± 0.022	1.307 ± 0.009	1.074 ± 0.011	0.233 ± 0.014	2.129 ± 0.026	1.982 ± 0.032	0.800 ± 0.013
K	1.100 ± 0.002	1.097 ± 0.002	1.016 ± 0.001	2.399 ± 0.018	1.342 ± 0.007	1.065 ± 0.009	0.277 ± 0.011	2.122 ± 0.021	1.993 ± 0.026	0.809 ± 0.011
N[i]	1.093 ± 0.005	1.077 ± 0.002	1.020 ± 0.001	2.384 ± 0.021	1.317 ± 0.007	1.069 ± 0.009	0.248 ± 0.011	2.136 ± 0.024	1.998 ± 0.028	0.813 ± 0.011

[a] States are shown in Scheme 1. [b] Normalized fluorescence values starting from $gp45^H$ equal to 1.0, where the superscript indicates the excitation wavelength and the subscript indicates which mutant was used in the measurement [V162C/W198F−CPM (AD) or W91F/V162C/W198F−CPM (A)]. [c] Determined by multiplying F_{AD}^{290} by the starting $I_{AD} + X$ value (2.166 ± 0.016, as determined for state H from Table 2). [d] X is the amount of interprotein FRET (from gp44/62 and/or gp43 tryptophans to CPM on gp45). [e] Determined by multiplying F_{A}^{290} by the starting $I_A + X$ value (1.186 ± 0.006, as determined for state H from Table 2). [f] Determined by multiplying F_{A}^{390} by the starting I_A value (1.048 ± 0.009, as determined for state H from Table 2). [g] Starting state assumed equal to 1.0. [h] No changes were observed from the previous state. [i] Determined from gp45, gp44/62, ATP, DNA, and gp43 versus EDTA.

Table 4: Energy-Transfer Efficiencies and W91 to V162C−CPM Distances of the Open gp45 Subunit Interface for the Intermediate State of Holoenzyme Assembly

assembly state[a]	E_T[b]	R (Å)[c]
A	0.692	40
B	0.692	40
C	0.688 ± 0.010	41[d]
D	0.622 ± 0.005	>45[e]
E	0.622 ± 0.005	>45[e]
F	0.741 ± 0.016	35
G	0.767 ± 0.010	33
H	0.745 ± 0.010	35
I	0.745 ± 0.010	35
J	0.800 ± 0.013	31
K	0.809 ± 0.011	30
L	0.760 ± 0.004	34
M	0.762 ± 0.010	33
N	0.813 ± 0.011	30
gp45·gp43	0.806 ± 0.019	31

[a] States are shown in Scheme 1. [b] Average energy transfer for all three W91/V162C−CPM pairs; the two W91/V162C−CPM pairs on the closed gp45 subunit interfaces are assumed to have constant energy transfer efficiencies of 0.95 (*22*). [c] Distance between W91 and V162C−CPM on the one open gp45 subunit interface, calculated by first determining the energy-transfer efficiency of the open subunit interface (E_O) by eq 4 [assuming E_C equal to 0.95 (*22*)] and then calculating R by eq 2. W91 and V162C are not the closest amino acids across the open subunit interface, and as such the distance between the closest amino acids across the open subunit interface [28 Å for our previous model of state A (*22*)] will be lower than the values presented here. [d] Values are for the first change in FRET for gp45 versus gp44/62 and ATP, rather than for gp45 versus gp44/62. [e] These distances are greater than $1.45R_0$, the upper limit for accurate measurement of distances by FRET (*26*).

and 10 mM magnesium acetate). The contents of syringe A were thus diluted by half, and the initial fluorescence value was obtained. The voltage on the photomultipier tube was adjusted to give a signal of −4 V for the initial fluorescence in all cases (the photomultiplier tube voltages required to yield −4 V were different for excitation at 290 and 390 nm). No changes in fluorescence were obtained over the course of the data collection, indicating that dilution did not cause dissociation of the gp45 trimer into monomers, which would cause a decrease in FRET, or that gp45 tryptophan or CPM was undergoing photobleaching. The buffer in syringe B was then replaced with the components indicated in the text or figure legends. Fluorescent changes were observed upon mixing syringes A and B. Data were collected at both 290 and 390 nm excitation wavelengths for each set of experiments. Several traces (between 3 and 9) at a single excitation wavelength were averaged to improve the signal-to-noise ratio, and the software provided by the manufacturer was used to fit the data to one, two, or three exponential processes as appropriate to obtain observed fluorescence amplitudes and rate constants. Following data collection, complex buffer was placed in both syringes and passed through the observation cell until the fluorescence decreased to a constant background value.

From these measurements, normalized fluorescence values in the presence (F_{AD}) and absence (F_A) of donor tryptophans were then calculated by dividing the background-subtracted final fluorescence by the background-subtracted initial fluorescence. Two mutants were used to determine these values: F_{AD} was determined using V162C/W198F and F_A using W91F/V162C/W198F, with superscripts indicating the excitation wavelength (290 or 390 nm).

As an example, V162C/W198F−CPM in complex buffer was placed in syringe A and mixed with complex buffer with excitation at 290 nm. The photomultiplier tube voltage was adjusted such that a signal of −4 V was obtained. gp44/62 in complex buffer was then placed in syringe B and mixed with syringe A, obtaining a final voltage of −4.22 V (−4 V plus or minus the fluorescence amplitude; larger negative numbers indicate increases in fluorescence). Complex buffer was then placed in both syringes and washed through the observation cell, yielding a background voltage of −0.50 V. The F_{AD}^{290} value is therefore equal to 1.063. The normalized fluorescence values are independent of the extent of acceptor labeling (gp45 is completely "labeled" with donor tryptophans; V162C/W198F−CPM samples with 0.3−1.7 CPM labels per trimer always yielded the same normalized fluorescence within experimental error; data not shown) and assumes the initial fluorescence of the starting state (found when the fluorophore was mixed with complex buffer described above at the beginning of data collection) is 1.0. The normalized fluorescence values (F_{AD}^{290}, F_{A}^{290}, and F_{A}^{390}) are reported in Tables 1−3 for the three multistep processes leading to holoenzyme formation.

Scheme 1

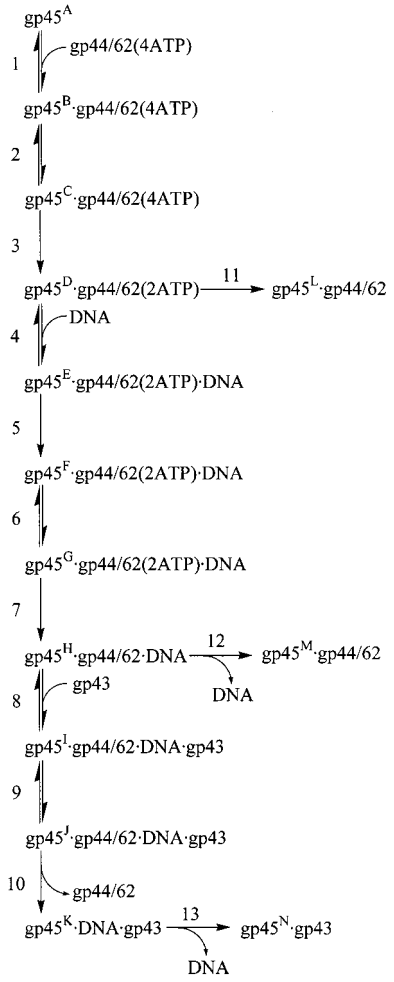

Since we are not collecting intensity data in the stopped-flow experiments, we use the normalized fluorescence values obtained above to modify the I_{AD} and I_A values of a reference state (a state where these parameters can be determined absolutely, such as by using steady-state fluorescence to obtain values for gp45 in complex buffer; the reference states used were the stable intermediate states A, D, and H from Scheme 1, see below) to yield I_{AD} and I_A values for the intermediate states of holoenzyme assembly. The F_{AD}^{290} and F_A^{290} values should be directly related to I_{AD} and I_A, respectively. However, we have found that F_{AD}^{290} and F_A^{290} both contain a signal due to interprotein FRET from tryptophans on gp44/62 and/or gp43 to CPM-labeled gp45. The F_{AD}^{290} and F_A^{290} values are therefore directly related to $I_{AD} + X$ and $I_A + X$, where X is equal to the amount of interprotein FRET. The magnitude of X can be determined by taking the difference between F_{AD}^{290} and F_{AD}^{390}: the emission *intensity* of any isolated fluorophore changes with excitation wavelength, but the Stokes shift remains constant. The *normalized* emission spectra are therefore constant at all excitation wavelengths (*29*), and normalized changes in I_A can be measured at any excitation wavelength for an isolated fluorophore. Exciting at 390 nm eliminates any contribution from interprotein FRET, and F_{AD}^{390} is therefore directly related to I_A.

To determine I_{AD} and I_A values for the various transient states (given the letters A−N in Scheme 1) observed in our kinetics investigation without any contribution from interprotein FRET, the following calculations were employed. The F_{AD}^{290}, F_A^{290}, and F_A^{390} values determined for the various states of holoenzyme assembly (Tables 1−3) were multiplied by $I_{AD} + X$, $I_A + X$, and I_A, respectively, determined for a reference state (see below) to yield $I_{AD} + X$, $I_A + X$, and I_A, respectively, for the various states of holoenzyme assembly (Tables 1−3). The magnitude of X was determined by subtracting I_A from $I_A + X$, and finally I_{AD} was determined by subtracting X from $I_{AD} + X$. To determine $I_{AD} + X$, $I_A + X$, and I_A values for states B, C, D, and L, the $I_{AD} + X$, $I_A + X$, and I_A values determined for gp45 in the steady-state ($gp45^A$; 1.85, 1.0, and 1.0, respectively) were used as the reference state. For example, F_{AD}^{290}, F_A^{290}, and F_A^{390} values for state C were found to be 1.158, 1.252, and 1.054, respectively. Multiplying F_{AD}^{290} by 1.85 (the $I_{AD} + X$ reference state for $gp45^A$), F_A^{290} by 1.00 (the $I_A + X$ reference state for $gp45^A$), and F_A^{390} by 1.00 (the I_A reference state for $gp45^A$) yields 2.142, 1.252, and 1.054, respectively. Subtracting 1.054 from 1.252 yields X (0.198), and subtracting X from 2.142 yields I_{AD} (1.944). The $I_{AD} + X$, $I_A + X$, and I_A values determined for $gp45^D$ above (and verified in the steady state; see below) were used as reference states for states E, F, G, H, and M, and the $I_{AD} + X$, $I_A + X$, and I_A values determined for $gp45^H$ above (and verified in the steady-state; see below) were used as reference states for states I, J, K, and N. Because of the possibility of accumulated errors in these measurements, the I_{AD}/I_A ratios for states D, H, and K were independently measured in the steady state, yielding 1.715 ± 0.085, 1.841 ± 0.092, and 2.004 ± 0.106, respectively, all of which are within experimental error of the stopped-flow measurements (average deviation of 2.4% from stopped-flow measurements).

The transfer efficiencies shown in Tables 1−3 for the various intermediate states of gp45 during holoenzyme assembly were then determined from eq 1 to yield a total energy transfer efficiency (E_T) for the three gp45 subunit interfaces. The total energy transfer is the average of all three subunit interfaces in each gp45 trimer, where E_O and E_C are the energy transfer efficiencies of the open and closed subunit interfaces, respectively. We have previously assumed that two of the three gp45 subunits are closed with $E_C = 0.95$, and that the total transfer efficiency is related to the transfer efficiencies of the open and closed subunit interfaces as follows (*22*):

$$E_O = 3E_T - 2E_C \quad (4)$$

assuming that the total energy transfer efficiency for multiple donor−acceptor pairs on a single protein (in this case three for gp45) is equal to the average transfer efficiency of the individual donor−acceptor pairs. Using E_O, the W91 to V162C−CPM distance for the open gp45 subunit interface can then be calculated from eq 2. The W91 to V162C−CPM distances for the various states of holoenzyme assembly for the one open gp45 subunit interface are shown in Table 4.

Determination of K_d Values. K_d values were determined by fitting the plot of F_{AD} or F_A versus protein concentration (gp44/62 or gp43) with KaleidaGraph (Synergy Software,

Table 5: ATPase Rates for ATP-γ-S.

conditions	observed rate (nM s^{-1})[a]
1 mM ATP-γ-S + 250 nM gp44/62 + 250 nM gp45	4[b]
+ 1 mM ATP	9
+ 2 mM ATP	14
1 mM ATP + 250 nM gp44/62 + 250 nM gp45	21
250 μM ATP-γ-S + 250 nM gp44/62 + 250 nM gp45 + 250 nM DNA	4[b]
+ 2.5 mM ATP	170
+ 5 mM ATP	223
1 mM ATP + 250 nM gp44/62 + 250 nM gp45 + 250 nM DNA	346

[a] The coupled spectrophotometric ATPase assay is described in detail elsewhere (*19*). The reproducibility of the data is about ±10%. Different stocks of DNA tend to give different observed rates (*13*). [b] Equal to the background rate of NADH oxidation.

Reading, PA) to the following quadratic equation:

$$F_{AD} \text{ or } F_A = 1 + \left(\frac{F_{max} - 1}{A_T}\right) \left(\frac{(A_T + B_T + K_d) - \sqrt{(A_T + B_T + K_d)^2 - 4A_T B_T}}{2}\right) \quad (5)$$

where F_{max} is the maximum normalized fluorescence (achieved upon saturation), A_T is the total concentration of gp45 (constant), and B_T is the total concentration of gp44/62 or gp43 (varied).

ATPase Assay. The coupled spectrophotometric ATPase assay was conducted as previously described (*5*, *19*). The ability for ATP to displace ATP-γ-S from gp44/62 was investigated as follows: 250 nM gp45, 250 nM gp44/62, and ATP-γ-S (with or without 250 nM DNA) were incubated, and the rate of hydrolysis was measured (presumably due entirely to background NADH oxidation). ATP was then added in aliquots, and the new rate of hydrolysis measured. Addition of ATP and mixing took about 30 s, and a new steady-state ATPase rate was achieved within 1 min of ATP addition. Observed rates of ATP hydrolysis are shown in Table 5.

Simulation of Holoenzyme Assembly and Disassembly. Stopped-flow FRET traces (V162C/W198F−CPM with excitation at 290 nm) were simulated using the PC version of KinSim or KinTekSim version 2.03 (*30*) using the mechanism shown in Scheme 1 and the parameters listed in the figure legends (taken from Tables 1−3 and 6). The simulated rate constants were optimized and then individually varied to determine how important their exact values were to the quality of the simulation. Table 6 shows the ranges over which the individual rate constants yielded satisfactory simulations. Steps were considered to be irreversible when inclusion of a reverse rate constant decreased the quality of the simulation regardless of its value.

RESULTS AND DISCUSSION

Investigating the Kinetics of gp45 Opening and Closing. We have used the gp45 mutants V162C/W198F and W91F/V162C/W198F to follow the opening and closing of the gp45 ring during the bacteriophage T4 DNA polymerase holoenzyme assembly process. The V162C and W91 positions are located on opposite sides of the gp45 subunit interface, and a FRET signal has been observed previously between these two amino acids when V162C was labeled with an appropriate fluorophore (*22*, *31*). The other gp45 tryptophan (W198) was mutated to a nonfluorescent phenylalanine to simplify the interpretation of the FRET data. In some cases, the W91F/V162C/W198F mutant was used to provide a gp45 mutant free of fluorescent tryptophan. We have previously used the V162C/W198F mutant labeled with the fluorescent acceptor coumarin (CPM) to determine that gp45 is an open trimer in solution, having one open subunit interface with a W91 to V162C−CPM distance of 35−38 Å and two closed subunit interfaces with W91 to V162C−CPM distances of 19 Å (*22*). W91 and V162C are not the closest amino acids across the subunit interface. Our previous model of gp45 open in solution (*22*) places the closest amino acid side chains about 28 Å apart across the open subunit interface. In the present study, we have observed the changes in the W91 to V162C−CPM FRET signal upon interaction with other holoenzyme components to develop a kinetic scheme for the holoenzyme assembly process (see Scheme 1; the distinct states observed during the holoenzyme assembly process have been assigned the letters A−N, while the kinetic steps leading between these states have been given the numbers 1−13) and measure the W91 to V162C−CPM distance of the open gp45 subunit interface during and after holoenzyme assembly. We have observed more intermediate steps than were observed in a previous study using gp45 labeled with an environmentally sensitive fluorescent probe (*15*).

Equations 1, 2, and 4 were used to determine W91 to V162C−CPM distances of the open gp45 subunit interface for the intermediate states during holoenzyme assembly, requiring the measurement of I_{AD} and I_A, the fluorescence intensities of the acceptor (CPM) in the presence and absence, respectively, of the donor (W91) upon excitation of the donor (290 nm). V162C/W198F−CPM and W91F/V162C/W198F−CPM were used to determine I_{AD} and I_A, respectively. However, tryptophans from gp44/62 and gp43 were found to contribute a small amount of interprotein FRET. Three measurements were therefore necessary to determine I_{AD} and I_A without any contributions from interprotein FRET: F_{AD}^{290}, the normalized change in fluorescence for V162C/W198F−CPM excited at 290 nm, F_A^{390}, the normalized change in fluorescence for W91F/V162C/W198F−CPM excited at 290 nm, and F_A^{390}, the normalized change in fluorescence for W91F/V162C/W198F−CPM excited at 390 nm. These three terms were converted to $I_{AD} + X$, $I_A + X$, and I_A, respectively, where X is the amount of interprotein FRET, and I_{AD} and I_A found by the appropriate subtraction (see Experimental Procedures). We have assumed that the W91 to V162C−CPM distances across the two closed gp45 subunit interfaces (19 Å) as well as the transfer efficiencies of these two closed subunit interfaces (0.95) are unchanged during the holoenzyme process, and therefore, all changes in transfer efficiency and W91 to V162C−CPM distance are attributed to the one open gp45 subunit interface.

Interaction of gp45 and gp44/62 in the Absence of ATP. The first step of the holoenzyme assembly process, interaction of gp45 and gp44/62, was investigated by stopped-flow FRET as shown in Figure 1A. Syringe A, containing 2 μM

Table 6: Holoenzyme Assembly and Disassembly Simulation Parameters

step[a]	process	forward rate constant[b]	reverse rate constant[b]
1	$gp45^{A} + gp44/62 \leftrightarrow gp45^{B}\cdot gp44/62$	$150-200\ \mu M^{-1}\ s^{-1}$	$65-85\ s^{-1}$
2	$gp45^{B}\cdot gp44/62 \leftrightarrow gp45^{C}\cdot gp44/62$	$100-110\ s^{-1}$	$50-60\ s^{-1}$
3[c]	$gp45^{C}\cdot gp44/62 \rightarrow gp45^{D}\cdot gp44/62$	$5.5-6.0\ s^{-1}$	*d*
4	$gp45^{D}\cdot gp44/62 + DNA \leftrightarrow gp45^{E}\cdot gp44/62\cdot DNA$	$60-80\ \mu M^{-1}\ s^{-1}$	$2-5\ s^{-1}$
5	$gp45^{E}\cdot gp44/62\cdot DNA \rightarrow gp45^{F}\cdot gp44/62\cdot DNA$	$175-225\ s^{-1}$	*d*
6	$gp45^{F}\cdot gp44/62\cdot DNA \leftrightarrow gp45^{G}\cdot gp44/62\cdot DNA$	$4.0-4.5\ s^{-1}$	$0.25-0.50\ s^{-1}$
7[c]	$gp45^{G}\cdot gp44/62\cdot DNA \rightarrow gp45^{H}\cdot gp44/62\cdot DNA$	$0.25-0.30\ s^{-1}$	*d*
8	$gp45^{H}\cdot gp44/62\cdot DNA + gp43 \leftrightarrow gp45^{I}\cdot gp44/62\cdot DNA\cdot gp43$	$400-600\ \mu M^{-1}\ s^{-1}$	$10-30\ s^{-1}$
9	$gp45^{I}\cdot gp44/62\cdot DNA\cdot gp43 \leftrightarrow gp45^{J}\cdot gp44/62\cdot DNA\cdot gp43$	$300-500\ s^{-1}$	$15-35\ s^{-1}$
10	$gp45^{J}\cdot gp44/62\cdot DNA\cdot gp43 \rightarrow gp45^{K}\cdot DNA\cdot gp43 + gp44/62$	$10-20\ s^{-1}$	*d*
11	$gp45^{D}\cdot gp44/62 \rightarrow gp45^{L}\cdot gp44/62$	$0.3-0.4\ s^{-1}$	*e*
12	$gp45^{H}\cdot gp44/62\cdot DNA \rightarrow gp45^{M}\cdot gp44/62 + DNA$	$0.10-0.15\ s^{-1}$	*e*
13	$gp45^{K}\cdot DNA\cdot gp43 \rightarrow gp45^{N}\cdot gp43 + DNA$	$0.01-0.05\ s^{-1}$	*e*

[a] Steps are shown in Scheme 1. [b] Data ranges indicate values that yield a satisfactory simulation. Values outside these ranges significantly affect the quality of the simulation. [c] ATP hydrolysis assigned to this step. [d] Irreversible; including a reverse rate constant always decreased the quality of the simulation. [e] Assumed to be irreversible.

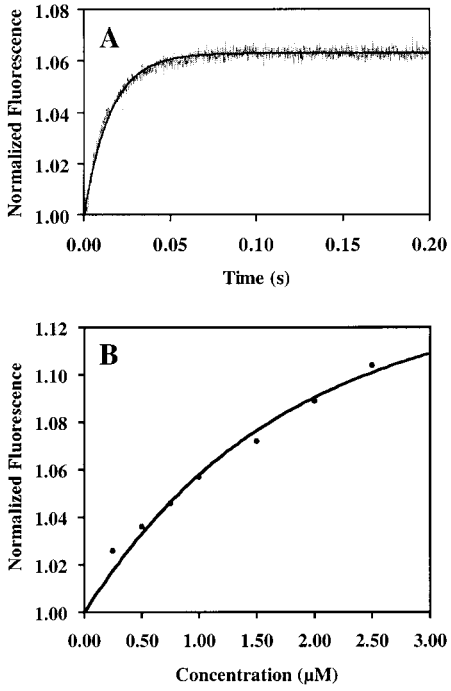

FIGURE 1: Interaction of gp45 and gp44/62 in the absence of ATP. (A) Stopped-flow FRET data (light line) of 2 μM V162C/W198F−CPM versus 2 μM gp44/62 in complex buffer with an excitation wavelength of 290 nm. The dark line is a fit to a single-exponential process yielding an observed rate constant of $70 \pm 16\ s^{-1}$. (B) Normalized fluorescence versus final gp44/62 concentration after mixing. Data (circles) were fit (line) using eq 5 to yield a maximum fluorescence of 1.166 ± 0.032 and a K_d of 1.2 ± 0.6 μM.

V162C/W198F−CPM in complex buffer, and syringe B, containing 2 μM gp44/62 in complex buffer, were mixed in a stopped-flow reaction analyzer in fluorescence mode with the excitation wavelength set at 290 nm and emission detected using a 420-nm cutoff filter such that only CPM fluorescence was observed (from FRET and direct CPM fluorescence). Mixing caused the contents of the two syringes to be diluted by half to 1 μM. The CPM fluorescence was seen to increase with an observed rate constant of $70 \pm 16\ s^{-1}$ (see Table 1 in Supporting Information for a full listing of observed kinetic parameters) and a normalized fluorescence (F_{AD}^{290}, see Experimental Procedures) of 1.063 ± 0.007 [assuming F_{AD}^{290} of the starting state, V162C/W198F−CPM in complex buffer ($gp45^{A}$, Scheme 1), is 1.0]. Altering the concentration of gp44/62 caused very little change in the observed rate constant (values between 59 and 78 s^{-1} over the range of 0.25−2.5 μM final gp44/62 concentration), but the normalized fluorescence increased with increasing gp44/62 concentration (see Figure 1B). Likewise, increasing the V162C/W198F−CPM concentration did not change the observed rate constant, confirming the first-order kinetic nature of the change in CPM fluorescence. The normalized fluorescence versus gp44/62 concentration plot was fit to eq 5, yielding an observed K_d of 1.2 ± 0.6 μM and a maximum normalized fluorescence (F_{max}) of 1.166 ± 0.032 (the fluorescent parameters reported here for gp45 and gp44/62 interacting in the absence of ATP are not listed in Table 1, although the $gp45^{C}$ parameters listed there for gp45 and gp44/62 interacting in the presence of ATP represent an analogous state). The $I_{AD} + X$ value for this process is 2.157 ± 0.059 [the product of $I_{AD} + X$ for $gp45^{A}$ determined in the steady state (1.85) and 1.166; see Experimental Procedures]. It has been previously shown by photo-cross-linking that gp45 and gp44/62 interact without the requirement for ATP (*32*).

The insensitivity of the observed rate constant to the gp44/62 and V162C/W198F−CPM concentrations suggests that the initial gp44/62 binding event (step 1, Scheme 1, leading to $gp45^{B}$ but in the absence of ATP) is faster than a subsequent conformational change first order in the $gp45^{B}\cdot$gp44/62 complex (step 2, Scheme 1, leading to $gp45^{C}$ but in the absence of ATP). To verify this suggestion, we simulated steps 1 and 2 of Scheme 1 using the program KinSim (*30*). The kinetic parameters were those found below for simulation of V162C/W198F−CPM versus gp44/62 and ATP ($k_1 = 175\ \mu M^{-1}\ s^{-1}$, $k_{-1} = 75\ s^{-1}$, $k_2 = 105\ s^{-1}$, and $k_{-2} = 55\ s^{-1}$; see Table 6) and fluorescent parameters found above ($gp45^{A} = 1.000$, $gp45^{B} = 1.000$, and $gp45^{C} = 1.166$). The gp45 concentration was held constant at 1 μM, while the gp44/62 concentration was varied from 0.25 to 2.5 μM. Fitting the simulated data the same way as the experimental data were fit above yielded observed rate constants from 74 to 97 s^{-1}, matching the behavior of the experimental data.

The changes in the $I_A + X$ and I_A terms during this process were investigated by using the W91F/V162C/W198F−CPM mutant and repeating the above experiment. Very similar observed rate constants (see Table 1, Supporting Information)

to those above were obtained with excitation at either 290 or 390 nm (to determine $I_A + X$ and I_A, respectively). The $I_A + X$ value was found to be 1.241 ± 0.020, while the I_A value was found to be 1.059 ± 0.003. The X and I_{AD} values for gp45^C in the absence of ATP were therefore found to be 0.182 ± 0.020 and 1.975 ± 0.062, respectively, and the I_{AD}/I_A ratio was found to be 1.865 ± 0.059. The changes in fluorescence leading to gp45^C are therefore due entirely to changes in interprotein FRET (from gp44/62 tryptophans) and changes in CPM environment rather than changes in intraprotein FRET (from W91 on gp45 to V162C−CPM), and the W91 to V162C−CPM distance is nearly unchanged (39 rather than 40 Å). The change in CPM fluorescence in step 2 may be due to a conformational change in gp44/62 that leads to movement of gp44/62 tryptophans relative to CPM on gp45.

Interaction of gp45 and gp44/62 in the Presence of ADP or ATP-γ-S. The experiment above with V162C/W198F−CPM and gp44/62 was repeated except that syringe B also contained 2 mM ADP or ATP-γ-S. Neither of these nucleotides are hydrolyzed by gp44/62, but gp44/62 has been shown to bind nonhydrolyzable analogues of ATP (*20*). For both mutants (excitation at 290 and 390 nm) and both nucleotides, similar first-order increases in CPM fluorescence were observed as without nucleotides. The observed rate constants and maximum changes in CPM fluorescence were very similar to those for gp44/62 in the absence of ATP as reported above (see Table 1, Supporting Information).

Interaction of gp45 and gp44/62 in the Presence of ATP. When syringe B contained 2 mM ATP, the results of the above experiments were very different. For the V162C/W198F−CPM mutant, the initial increase in CPM fluorescence was observed, but a subsequent decrease in CPM fluorescence was also observed (Figure 2A). Mixing 2 μM each V162C/W198F−CPM and gp44/62 with ATP yielded observed rate constants of 81 ± 19 and 3.6 ± 1.0 s^{-1}, with a normalized fluorescence value (F_{AD}^{290}) for the first change (step 2, Scheme 1) of 1.066 ± 0.007, and a normalized fluorescence value of the second change (step 3, Scheme 1) of 0.996 ± 0.007 (both starting from 1.0). Altering the gp44/62 concentration did not change either of the two observed rate constants, but as before, the normalized fluorescence of the first change in CPM fluorescence increased with increasing gp44/62 concentration (Figure 2B). The normalized fluorescence values for the first change in CPM fluorescence were fit to eq 5 yielding an observed K_d of 0.59 ± 0.17 μM and F_{max} of 1.158 ± 0.013 (see Table 1). This K_d value is similar to the one determined above in the absence of ATP (1.2 μM). The second change in normalized fluorescence for V162C/W198F−CPM versus gp44/62 and ATP, however, was not altered with different gp44/62 concentrations (0.999 ± 0.006 for six gp44/62 concentrations from 0.25 to 2.5 μM), suggesting that gp45 was quantitatively converted to this second new conformational state (gp45^D, Scheme 1). Doubling the V162C/W198F−CPM concentration did not change either of the observed rate constants, confirming that both changes in CPM fluorescence were first-order. We chose not to decrease the V162C/W198F−CPM concentration because we were concerned that at lower concentrations gp45 would begin to dissociate into monomers [we have found the cooperative dissociation constant for gp45 trimers to be 0.08−0.21 μM^2 (*22*, *31*)] and complicate FRET-based distance measurements. A previous investigation measuring changes in fluorophore environment on gp45 during the holoenzyme assembly process found that at 250 nM gp45, varying the gp44/62 concentration yielded changes in the observed rate constants (*15*). The $I_{AD} + X$ values for states C and D were found to be 2.142 ± 0.020 and 1.848 ± 0.011. The absolute requirement for ATP to observe the second change in CPM fluorescence suggests that ATP hydrolysis is occurring in this step (step 3, Scheme 1).

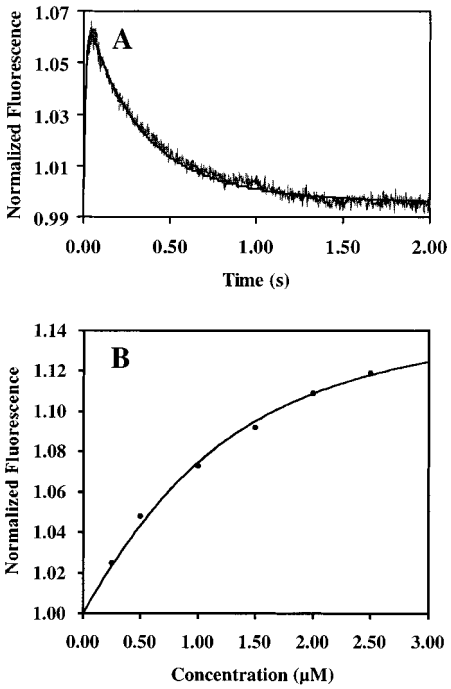

FIGURE 2: Interaction of gp45 and gp44/62 in the presence of ATP. (A) Stopped-flow FRET data (light line) of 2 μM V162C/W198F−CPM versus 2 μM gp44/62 and 2 mM ATP in complex buffer with an excitation wavelength of 290 nm. The dark line is a simulation using steps 1−3 and 11 of Scheme 1, kinetic parameters from Table 6 (k_1 = 150−200 μM^{-1} s^{-1}, k_{-1} = 65−85 s^{-1}, k_2 = 100−110 s^{-1}, k_{-2} = 50−60 s^{-1}, k_3 = 5.5−6.0 s^{-1}, and k_{11} = 0.3−0.4 s^{-1}), and fluorescent parameters from Table 1 (gp45^A = 1.000, gp45^B = 1.000, gp45^C = 1.158, gp45^D = 0.999, and gp45^L = 1.152). (B) Normalized fluorescence versus final gp44/62 concentration after mixing. Data (circles) were fit (line) using eq 5 to yield a maximum fluorescence of 1.158 ± 0.013 and a K_d of 0.59 ± 0.17 μM.

When this experiment was performed with W91F/V162C/W198F−CPM with excitation at 290 nm, two changes in normalized fluorescence were observed as before, with the amplitude of the first change in CPM fluorescence larger than the second. The observed kinetics were very similar to those observed above for V162C/W198F−CPM (see Table 1, Supporting Information). The I_{AD}/I_A ratios for states C and D (see Scheme 1) were found to be 1.844 ± 0.028 and 1.763 ± 0.015 (see Table 1). As was observed for gp45^C in the absence of nucleotides, gp45^C in the presence of ATP and gp45^A have nearly identical distances across their open subunit interfaces (41 versus 40 Å), but gp45^D has had its subunit interface opened to a distance larger than in gp45^A [>45 Å, see Table 4; the open subunit interface distance is greater than 1.45R_0, the upper limit for accurate measurement of distances by FRET (*26*)]. gp44/62 has coupled ATP hydrolysis to gp45 ring opening in the step preceding interaction with DNA.

The stopped-flow data for V162C/W198F−CPM excited at 290 nm (F_{AD}^{290}) were simulated using the mechanism shown in Scheme 1 to obtain forward and reverse rate constants, K_d values, and K_{eq} values (see Table 6). This data set was chosen because it contains the largest amount of fluorescent information (changes in interprotein and intraprotein FRET as well as changes in CPM fluorescence). All of the experimental data were successfully fit with the mechanism shown in Scheme 1. Since the initial binding events were often not observed by fluorescence, steps were added to the mechanism (1, 4, and 8) to include these events. The simulated rate constants were all close to the observed rate constants except when an observed rate constant included a binding event and a first-order conformational change. However, the simulated K_d values obtained for the binding events were close to current or previous experimental data.

We have found that gp45 and gp44/62 bind with a simulated K_d of about 0.4 μM (step 1, Scheme 1), similar to the observed K_d value determined above by eq 5 for gp45 and gp44/62 in the presence of ATP, in a process that does not cause a change in CPM fluorescence or the W91 to V162C−CPM distance. A subsequent conformational change in the gp45·gp44/62 complex does not appreciably change the W91 to V162C−CPM distance (40−41 Å; step 2, Scheme 1). Simulations found that this change is reversible, with a K_{eq} of about 2.0 ($k_{forward}$ of 100−110 s^{-1}, similar to the observed rate constant for the first change in CPM fluorescence for gp45 versus gp44/62 and ATP). The nonhydrolyzable ATP analogues ADP or ATP-γ-S did not cause further changes in CPM fluorescence, but ATP causes a decrease in CPM fluorescence with a simulated rate constant of 5.5−6.0 s^{-1} (step 3, Scheme 1), similar to the observed value of 3.6 s^{-1}. We assign this process to ATP hydrolysis on the basis of the requirement for a hydrolyzable form of ATP, the simulation showing that this step is irreversible, and the similarity of this rate constant to the previously determined burst rate of 5 s^{-1} for ATP hydrolysis by gp44/62 in the presence of gp45 (*15*). Two of the four total ATP molecules hydrolyzed by gp44/62 during holoenzyme assembly are hydrolyzed at this step (*15*). The gp45 ring is reopened to a W91 to V162C−CPM distance of >45 Å concomitant with ATP hydrolysis. The further opening of the gp45 ring may be required to allow DNA to pass into the center of the gp45 ring in the next step of holoenzyme assembly.

Formation of a gp45·gp44/62·DNA Complex. The $gp45^{D}$·gp44/62 complex (formed in the presence of 2 mM ATP) was placed in syringe A and mixed with DNA [the forked bio62/34/36 primer-template blocked with streptavidin used previously (*5*, *19*)] placed in syringe B. Three processes were observed when V162C/W198F−CPM was excited at 290 nm: two increases in CPM fluorescence followed by one decrease in CPM fluorescence (see Figure 1, Supporting Information, for fits of two and three exponential processes to these data, as well as Figure 3 for simulation of these data as described below). The observed rate constants were 23 ± 2, 2.9 ± 0.3, and 0.31 ± 0.09 s^{-1} when 2 μM $gp45^{D}$·gp44/62 with 2 mM ATP and 2 μM DNA were mixed (see Table 2, Supporting Information). The first rate constant was found to depend on the DNA concentration: doubling the DNA concentration caused an increase to 51 ± 4 s^{-1}, while halving the DNA concentration caused a decrease to 13 ± 1 s^{-1} (observed second-order rate constant of 25 ± 2 μM^{-1} s^{-1}). The apparent second-order nature of the first change in CPM fluorescence suggests that it is due either to DNA binding or that DNA binding is limiting the observed rate constant of a subsequent conformational change. Kinetic simulations favor the latter explanation (see below). Curiously, the normalized fluorescence values (F_{AD}^{290}) of this first change in CPM fluorescence were unchanged for all three DNA concentrations, suggesting that multiple clamps were loaded onto a single DNA primer-template. Once the DNA concentration in syringe B was lowered below 500 nM, the normalized fluorescence began to decrease, suggesting that a maximum of four clamps could be loaded onto this DNA substrate. The site size of gp45 on DNA has previously been shown to be about 10 bp (*33*); the forked primer-template used in this study has 34 bp and 10 single-stranded bases between the biotin/streptavidin block and the DNA fork, which would be expected to accommodate the 4 clamps that were observed to be loaded onto this DNA substrate. The rate constants of the second and third changes in CPM fluorescence were not dependent on the DNA concentration, suggesting that they are first order and due to conformational changes.

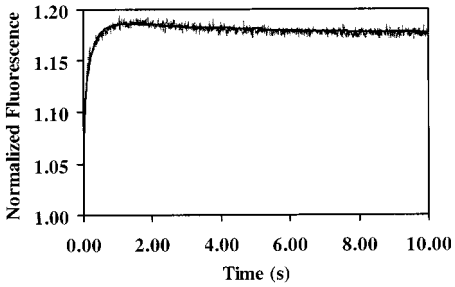

FIGURE 3: Interaction of $gp45^{D}$·gp44/62 complex formed in the presence of ATP with DNA. Stopped-flow FRET data (light line) of 2 μM V162C/W198F−CPM, 2 μM gp44/62, and 2 mM ATP versus 2 μM DNA in complex buffer with an excitation wavelength of 290 nm. The dark line is a simulation using steps 4−7 and 12 of Scheme 1, kinetic parameters Table 6 (k_4 = 60−80 μM^{-1} s^{-1}, k_{-4} = 2−5 s^{-1}, k_5 = 175−225 s^{-1}, k_6 = 4.0−4.5 s^{-1}, k_{-6} = 0.25−0.50 s^{-1}, k_7 = 0.25−0.30 s^{-1}, and k_{12} = 0.10−0.15 s^{-1}), and fluorescent parameters from Table 2 ($gp45^{D}$ = 1.000, $gp45^{E}$ = 1.000, $gp45^{F}$ = 1.130, $gp45^{G}$ = 1.200, $gp45^{H}$ = 1.180, and $gp45^{M}$ = 1.172).

Repeating these experiments with W91F/V162C/W198F−CPM yielded similar results. Exciting at 290 nm yielded three changes in CPM fluorescence (two increases followed by a decrease) with similar observed rate constants as above, while when exciting at 390 nm only the first two increases in CPM fluorescence were observed (see Table 2, Supporting Information). The I_{AD}/I_A ratios for states F, G, and H were found to be 1.909 ± 0.040, 1.941 ± 0.025, and 1.914 ± 0.025 (see Table 2), with W91 to V162C−CPM distances of 35, 33, and 35 Å (see Table 4), a sharp drop in distance from $gp45^{D}$.

Simulation of the V162C/W198F−CPM data showed that the DNA initially binds to the gp45·gp44/62 complex (step 4, Scheme 1) with a simulated K_d of about 50 nM ($k_{forward}$ of 60−80 μM^{-1} s^{-1}, see Table 6), consistent with a previous observation (*15*), without causing a change in CPM fluorescence or W91 to V162C−CPM distance (step 4, Scheme 1). Three subsequent conformational changes that altered the

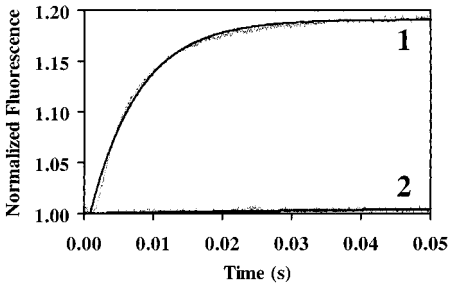

FIGURE 4: Interaction of gp45 and gp43. Stopped-flow FRET data (light lines) of 2 μM V162C/W198F−CPM versus (1) 2 μM gp43 or (2) 2 μM gp43Δ6 (a mutant missing the last six C-terminal amino acids) in complex buffer with an excitation wavelength of 290 nm. The dark lines are fits to single-exponential processes yielding observed rate constants of 142 ± 8 (gp43) and 18 ± 1 s^{-1} (gp43Δ6). Because of the rapid interaction of gp45 and gp43, the dead-time due to mixing (ca. 2 ms) can be seen at the beginning of the data collection.

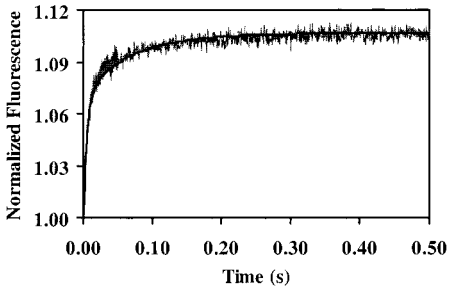

FIGURE 5: Formation of the holoenzyme. Stopped-flow FRET data (light line) of 2 μM V162C/W198F−CPM, 2 μM gp44/62, 2 mM ATP, and 2 μM DNA versus 2 μM gp43 in complex buffer with an excitation wavelength of 290 nm. The dark line is a simulation using steps 8−10 and 13 of Scheme 1, kinetic parameters from Table 6 (k_8 = 400−600 μM^{-1} s^{-1}, k_{-8} = 10−30 s^{-1}, k_9 = 300−500 s^{-1}, k_{-9} = 15−35 s^{-1}, k_{10} = 10−20 s^{-1}, and k_{13} = 0.01−0.05 s^{-1}), and fluorescent parameters from Table 3 ($gp45^H$ = 1.000, $gp45^I$ = 1.000, $gp45^J$ = 1.083, $gp45^K$ = 1.100, and $gp45^N$ = 1.093).

W91 to V162C−CPM distance of the open gp45 subunit interface were then observed, with simulated rate constants of 175−225 s^{-1} (step 5, Scheme 1), 4.0−4.5 s^{-1} (step 6, Scheme 1), and 0.25−0.30 s^{-1} (step 7, Scheme 1). Since step 4 is slower than step 5, only a rate-limiting second-order process was observed experimentally. The first exponential fit to the data (23 s^{-1} for 1 μM final $gp45^D$·gp44/62 and DNA; see Table 2, Supporting Information) is therefore a composite of the simulated rate constants for steps 4 and 5. However, the simulated rate constants for steps 6 and 7 are similar to the observed rate constants for the second and third changes in CPM fluorescence. Only the middle rate constant (step 6) required a reverse rate constant for successful simulation of the data. The rate constants for steps 6 and 7 bracket the burst rate of 1 s^{-1} for ATP hydrolysis by gp44/62 in the presence of gp45, DNA, and ATP (*15*, *19*), implicating these steps, particularly the irreversible step 7, as due to ATP hydrolysis. The binding of DNA triggers a subsequent conformational change and results in a contraction of the W91 to V162C−CPM distance of the open gp45 subunit interface to 35 Å, immediately followed by hydrolysis of ATP that leaves the W91 to V162C−CPM distance largely unchanged.

Interaction of gp45 and gp43. The ability of gp45 and gp43 to interact in the absence of gp44/62 or DNA was investigated by placing 2 μM V162C/W198F−CPM in complex buffer in syringe A and mixing with 2 μM gp43 in syringe B. A large increase in CPM fluorescence was found (Figure 4, curve 1) with an observed rate constant of 142 ± 8 s^{-1} and a normalized fluorescence (F_{AD}^{290}) of 1.193 ± 0.004. Changing either the gp43 or V162C/W198F−CPM concentration did not change the observed rate constant (see Table 3, Supporting Information), but increasing the concentration of gp43 increased the normalized fluorescence. Fitting the normalized fluorescence versus gp43 concentration plot to eq 5 yielded an observed K_d of 48 ± 27 nM and an F_{max} of 1.263 ± 0.010. The W91F/V162C/W198F−CPM mutant yielded similar observed kinetic parameters (see Table 3, Supporting Information). The I_{AD}/I_A ratio was found to be 1.989 ± 0.047 (see Table 1) with a W91 to V162C−CPM distance of 31 Å (see Table 4), indicating that the interaction of gp43 with gp45 causes a substantial conformational change that results in closure of the open gp45 subunit interface. The large amount of interprotein FRET (*X* equal to 0.267; see Table 1) indicates that gp43 and gp45 are likely to be arranged close together such that one gp43 tryptophan (or more) approaches V162C−CPM on gp45. The low K_d value, the substantial conformational change upon binding, and the large amount of interprotein FRET all suggest that gp45 and gp43 share a significant contact surface that is centered upon the interaction between the C-terminus of gp43 and the subunit interface of gp45.

Interaction of gp45 and gp43Δ6. The C-terminal tail of gp43 has previously been shown to be essential for forming the holoenzyme (*11*), and the C-terminal tail of gp43 has been shown to interact with the subunit interface of gp45 (*12*). A mutant of gp43 missing the last six amino acids (gp43Δ6) was investigated for its ability to interact with V162C/W198F−CPM. The same experiment as above with gp43 was conducted with 2μM V162C/W198F−CPM in complex buffer in syringe A and 2 μM gp43Δ6 in complex buffer in syringe B. Upon mixing, very little change in FRET was observed (normalized fluorescence of 1.007 ± 0.001; Figure 4, curve 2). This mutant of gp43 does not cause the open subunit interface of gp45 to close, providing additional evidence that the C-terminus of gp43 is interacting with the gp45 subunit interface.

Formation of the Holoenzyme. The final state of the holoenzyme was formed by placing 2 μM V162C/W198F−CPM, 2 μM gp44/62, 2 μM DNA, and 2 mM ATP in syringe A and mixing with 2 μM gp43 in syringe B. Two increases in CPM fluorescence were found (Figure 5), with observed rate constants of 93 ± 22 and 8.5 ± 2.0 s^{-1} (see Table 4, Supporting Information) and normalized fluorescence values (F_{AD}^{290}) of 1.083 ± 0.006 and 1.100 ± 0.002. Decreasing the concentration of gp43 did not change the observed rate constants, suggesting that they are due to first-order conformational changes, but it decreased the normalized fluorescence values of the changes in CPM fluorescence. With the W91F/V162C/W198F−CPM mutant excited at 290 nm, two increases in CPM fluorescence were observed, but interestingly, excitation at 390 nm yielded an increase followed by a decrease in CPM fluorescence. The I_{AD}/I_A values for states J and K were found to be 1.982 ± 0.032 and 1.993 ± 0.026 (see Table 3) with W91 to V162C−CPM distances of 31 and 30 Å (see Table 4). The final W91 to V162C−CPM distance of 30 Å is almost identical to the distance observed in the gp45·gp43 complex (31 Å). The holoeznyme (state

K, Scheme 1) has a significant amount of interprotein FRET (*X* equal to 0.277; see Table 3) and is also nearly equal to that found in the gp45·gp43 complex. As with the gp45·gp43 complex, gp45 in the holoenzyme has undergone substantial conformational reorganization relative to gp45 free in solution.

Since the C-terminus of gp43 has been suggested to be inserted into the subunit interface of gp45 (*12*), it is not surprising that gp45 in the holoenzyme is not completely closed (the W91 to V162C−CPM distance would then be 19 Å). The C-terminus of gp43 is largely unstructured in the X-ray crystal structure (*10*), but may become structured upon interaction with gp45. If it assumes an α-helix, for instance, the diameter of the C-terminus of gp43 would be 6 Å plus the distance covered by the side chains, easily accommodating the 11 Å difference between gp45 in the holoenzyme and a completely closed gp45 structure. The similarity of the W91 to V162C−CPM distance and the amount of interprotein FRET for the holoenzyme and the gp45·gp43 complex suggests that the protein−protein contacts within these complexes are similar, although the global conformations may change due to DNA binding. The precise spatial orientation of the holoenzyme awaits elucidation.

Simulation of the holoenzyme assembly data yielded a K_d for the interaction of the gp45^H·gp44/62·DNA complex with gp43 (step 8, Scheme 1) of about 40 nM (see Table 6) without a change in CPM fluorescence, followed by two steps that result in changes in CPM fluorescence. The first gp45 conformational change is reversible (step 9, Scheme 1), with a simulated $k_{forward}$ of 300−500 s^{-1}, and the second is irreversible (step 10, Scheme 1), with a simulated rate constant of 10−20 s^{-1} (similar to the observed rate constant of 8.5 s^{-1} for the second change in CPM fluorescence). Since we find step 10 to be irreversible and associated with a decrease in F_A^{390}, we assign this step to the disassociation of gp44/62. In step 2 of holoenzyme assembly (the first conformational change when gp45 interacts with gp44/62), there is an increase in I_A that only decreases in steps 3 and 10. gp44/62 certainly does not dissociate in step 3, so the decrease in I_A in step 10 suggests that gp44/62 departure is relieving a previously imposed increase in I_A. Proof of this assignment will require additional experiments, perhaps using fluorescent labels attached to gp44/62 or by fluorescence polarization.

Breakdown of the gp45^D·gp44/62 Complex. The gp45^D·gp44/62 complex formed in the presence of ATP was mixed with EDTA to follow its breakdown. EDTA complexes with magnesium and prevents the hydrolysis of ATP by gp44/62. A single increase in CPM fluorescence occurred upon mixing, with an observed rate constant of 0.36 ± 0.01 s^{-1} (step 11, Scheme 1; Figure 6). Changing the protein concentration did not cause a change in this observed rate constant. The I_{AD}/I_A ratio for gp45^L is 1.933 ± 0.009 (see Table 1), indicating that gp45 has closed to a W91 to V162C−CPM distance of 34 Å (see Table 4). Moving from state D to L causes an increase in the F_{AD}^{290}, F_A^{290}, and F_A^{390} terms, resulting in a decrease in the W91 to V162C−CPM distance as would be expected if the activated gp45^D·gp44/62 complex formed by ATP hydrolysis relaxed to a ground-state, gp45^C-like (pre ATP hydrolysis) gp45^L·gp44/62 complex when exposed to EDTA. ATP hydrolysis is required to maintain an activated form of the gp45·gp44/62 complex, as was observed previously (*13*, *14*). The F_A^{290} term does not change as much as expected, resulting in a shorter W91 to V162C−CPM distance than anticipated, suggesting that the gp45^L·gp44/62 complex is in a slightly different conformation than in the gp45^C·gp44/62 complex. The simulated rate constant of the breakdown of the gp45^D·gp44/62 complex (0.3−0.4 s^{-1}) was found to be identical with a previous study using an environmentally sensitive fluorophore (*15*) and is slower than any of the rate constants for the steps (1−3, Scheme 1) leading to formation of the complex, consistent with the burst of ATP hydrolysis observed previously with gp45, gp44/62, and ATP [since a step following chemistry is the rate-limiting step in the assembly and disassembly process (*15*)].

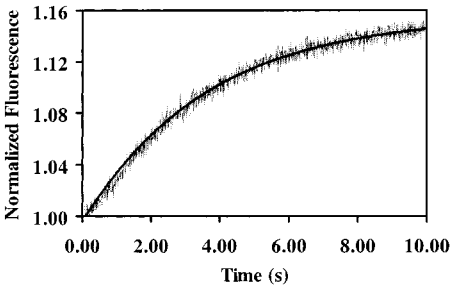

FIGURE 6: Breakdown of the gp45^D·gp44/62 complex formed in the presence of ATP. Stopped-flow FRET data (light line) of 2 μM V162C/W198F−CPM, 2 μM gp44/62, and 2 mM ATP versus 100 mM EDTA in complex buffer with an excitation wavelength of 290 nm. The dark line is a fit to a single-exponential process yielding an observed rate constant of 0.36 ± 0.01 s^{-1}.

Breakdown of the gp45^H·gp44/62·DNA Complex. The gp45^H·gp44/62·DNA complex formed in the presence of DNA was mixed with EDTA to follow its breakdown. Very little change in CPM fluorescence was observed for this process for V162C/W198F−CPM excited at 290 nm, and no change in CPM fluorescence was observed for W91F/V162C/W198F−CPM excited at 390 nm. Only W91F/V162C/W198F−CPM excited at 290 nm yielded significant changes in CPM fluorescence that allowed an observed rate constant of 0.05 ± 0.01 s^{-1} to be determined (data not shown). The simulated rate constant was found to be 0.10−0.15 s^{-1} (see Table 6), while the rate constant for this step was previously found to be 0.3 s^{-1} (*15*). The I_{AD}/I_A value of gp45^M·gp44/62 was found to be 1.935 ± 0.025 (see Table 2) with W91 to V162C−CPM distance of 33 Å (see Table 4), values very close to those for the gp45^L·gp44/62 complex. Likewise, the amount of interprotein FRET for states L and M are very close, further suggesting that the final states for both the gp45^D·gp44/62 and gp45^H·gp44/62·DNA complexes upon exposure to EDTA are indentical. The off rate of gp45 from DNA has the slowest rate constant in the overall gp45^H·gp44/62·DNA complex assembly and disassembly process and is consistent with the observation of a burst of ATP hydrolysis by gp44/62 in the presence of gp45, DNA, and ATP [since a step following chemistry is the rate-limiting step in the assembly and disassembly process (*15*, *19*, *20*)]. The simulated gp45 off rate is also consistent with the steady-state rate of ATP hydrolysis by gp44/62 for a mixture of gp45, gp44/62, and DNA (346 nM s^{-1}; see Table 5). Multiplying the simulated gp45 off rate by the gp44/62 concentration (250 nM) and four molecules of ATP hydro-

lyzed per assembly and disassembly cycle (*19*) yields 100−150 nM s^{-1}, comparable to the experimental rate.

Breakdown of the Holoenzyme. Placing 2 μM V162C/W198F−CPM, 2 μM gp44/62, 2 μM DNA, 2 μM gp43, and 2 mM ATP in syringe A and mixing with EDTA in syringe B yielded very little change (data not shown), similar to the breakdown of the gp45^{H}·gp44/62·DNA complex. The I_{AD}/I_A ratio for state N was found to be 1.998 ± 0.028 (see Table 3), and the W91 to V162C−CPM distance unchanged at 30 Å (see Table 4). The gp45·gp43 complex has an I_{AD}/I_A ratio of 1.989, suggesting that upon release from the holoenzyme and in the absence of ATP hydrolysis, gp45 forms a complex with gp43 rather than with gp44/62. The amount of interprotein FRET (*X* equal to 0.248; see Table 3) also suggests an interaction with gp43 rather than gp44/62. The observed K_d values determined above (43 nM and 1.2 μM for gp43 and gp44/62, respectively) are likewise consistent. Because of the small changes in CPM fluorescence, rate constants were difficult to assign to this step. Simulation yielded a rate constant of 0.01−0.05 s^{-1} (see Table 6) for the breakdown of the holoenzyme. The rate constant for this step has previously been shown to be between 0.002 and 0.03 s^{-1} (*5*, *13*, *34*). The simulated rate constant for breakdown of the holoenzyme is also consistent with the steady-state rate of ATP hydrolysis by gp44/62 for a mixture of gp45, gp44/62, DNA, and gp43 [about 10-fold lower than for a mixture of gp45, gp44/62, and DNA; 20 nM s^{-1} as previously reported (*19*)]. Multiplying the simulated rate constant for holoenzyme breakdown by the gp44/62 concentration (250 nM) and four molecules of ATP hydrolyzed per holoenzyme assembly and disassembly cycle (*19*) yields 10−50 nM s^{-1}, again comparable to the experimental rate.

Interaction of the gp45^{C}·gp44/62·ATP-γ-S Complex with DNA. The importance of ATP hydrolysis in forming the gp45^{H}·gp44/62·DNA complex was investigated by substituting ATP-γ-S for ATP. When 2 μM V162C/W198F−CPM, 2 μM gp44/62, and 2 mM ATP-γ-S were placed in syringe A and mixed with 2 μM DNA in syringe B, a decrease in CPM fluorescence was observed (data not shown) with an observed rate constant of 2.6 ± 0.3 s^{-1} and a normalized fluorescence of 0.964 ± 0.005 (starting from 1.0). The direction of the change in CPM fluorescence is opposite to that observed with ATP and suggests that a nonproductive complex has formed, indicating that ATP hydrolysis is necessary to form the gp45^{H}·gp44/62·DNA complex. Our measurements cannot determine whether DNA is part of the above complex formed with ATP-γ-S.

Competing gp44/62·ATP-γ-S with ATP. To investigate whether ATP-γ-S locks the gp45·gp44/62 complex into a stable, nonproductive form as is observed with the *E. coli* DNA replication system (*17*, *18*), we mixed the gp45·gp44/62·ATP-γ-S complex with 1 equiv of ATP (data not shown). An increase in CPM fluorescence was found, as would be expected for formation of the ATP hydrolysis-dependent gp45^{D}·gp44/62 complex, with an observed rate constant of 0.82 ± 0.02 s^{-1}. This was consistent with near quantitative formation of the gp45^{D}·gp44/62 complex: the normalized fluorescence was 1.025 ± 0.001 (assuming a starting value of 1.089, the end point of 2 μM V162C/W198F−CPM versus 2 μM gp44/62 and 2 mM ATP-γ-S), where 0.999 is the expected normalized fluorescence of gp45^{D}·gp44/62.

Further investigation made use of a coupled spectrophotometric ATPase assay (*19*), in which ATP hydrolysis is coupled to NADH oxidation and a change in absorbance at 340 nm. Complex buffer containing 250 nM wild-type gp45, 250 nM gp44/62, and 1 mM ATP-γ-S had a hydrolysis rate of 4 nM s^{-1} (see Table 5), equal to the background rate of NADH oxidation in complex buffer. Addition of 2 mM ATP resulted in a new steady-state ATPase rate of 14 nM s^{-1}, nearly equal to the ATPase rate of 250 nM gp44/62 in the presence of 250 nM gp45 and 1 mM ATP (21 nM s^{-1}). This new steady-state ATPase rate was achieved within 1 min of ATP addition.

The gp45·gp44/62·ATP-γ-S·DNA complex was also investigated for its ability to compete ATP-γ-S with ATP. Stopped-flow FRET yielded very little change in FRET when mixing 1 equiv of a gp45·gp44/62·ATP-γ-S·DNA complex with 1 equiv of ATP. The coupled spectrophotometric ATPase assay was much more insightful: 250 nM gp45, 250 nM gp44/62, 250 nM DNA, and 250 μM ATP-γ-S had a background rate of 4 nM s^{-1}, and upon addition of 2.5 mM ATP, the rate only increased to 170 nM s^{-1} (see Table 5; 250 nM gp45, 250 nM gp44/62, 250 nM DNA, and 1 mM ATP yielded a rate of 346 nM s^{-1}). Addition of 20 equiv of ATP yielded a rate of 223 nM s^{-1}, about two-thirds of the rate with ATP alone. As above, all of these new steady-state rates were achieved within 1 min of ATP addition. These observations are in contrast to what has been observed with the *E. coli* DNA replication system, where the γ complex can be trapped in a nonproductive form with ATP-γ-S that requires hours for ATP to be exchanged with ATP-γ-S (*18*).

CONCLUSIONS

In this paper, we have used stopped-flow FRET to investigate the opening and closing of the gp45 ring during bacteriophage T4 holoenzyme assembly. Assembly of the holoenzyme is an ordered process (*13*−*15*), and different assembly states (designated with the letters A−N in Scheme 1) can be observed by deleting one or more of the necessary components of the holoenzyme. The kinetic parameters of the assembly and disassembly process (the forward and reverse rate constants for steps 1−13 in Scheme 1) were determined by simulating the experimental stopped-flow traces, as shown in Figures 2, 3, and 5 and in Table 6. Good agreement was found between many of the assembly rate constants and all of the disassembly rate constants for this fluorescent method with previous kinetic measurements. Distances between W91 and V162C−CPM, two amino acids that lie on opposite sides of the gp45 subunit interface, for the open gp45 subunit interface in the various gp45 conformations during the assembly of the holoenzyme were determined according to eqs 1, 2, and 4 using the magnitude of the changes in CPM fluorescence (F_{AD}^{290}, F_{A}^{290}, and F_{A}^{390}) and are shown in Table 4.

The transfer efficiencies shown in Tables 1−4 are model independent, but the distances shown in Table 4 rest on an assumption about the values of the terms that comprise R_o (ϕ_D, κ^2, and *J*). Because of the tryptophans present in gp44/62 and gp43, the values of the terms comprising R_o cannot be determined for intermediate states of gp45 during holoenzyme assembly. Due to this limitation, we assume that

the values of R_o and its component terms calculated for CPM-labeled gp45 in complex buffer do not change during the holoenzyme assembly process, and as a result, these values have been used for determination of all intermediate W91 to V162C−CPM distances. The following data support this assumption. In state A, we have determined R_o to be 31 Å (*22*) and the W91 to V162C−CPM distance of the open gp45 subunit interface to be 40 Å (Table 4). If the W91 to V162C−CPM distance of the open subunit interface in the final holoenzyme complex (state K) is 40 Å as well, rather than 30 Å as shown in Table 4, R_o would then have to increase to 41 Å (using eq 4, the energy transfer efficiency of the open subunit interface for state K is 0.527, and using eq 2, R_o would need to be 41 Å to yield a W91 to V162C−CPM distance of 40 Å). The *J* term (overlap integral) cannot yield such a change in R_o: a 20-nm change in the tryptophan emission maximum (a change in the Stokes shift) only changes R_o by up to 1.5 Å, and moving to a more hydrophobic environment (as would be expected if in a multiprotein complex) actually *decreases* R_o. The quantum yield (ϕ_D) of tryptophan in a protein generally does not exceed 0.2 (*35*), and increasing to this value in the present case would only increase R_o by 2 Å. The κ^2 term is very difficult to directly measure (*26*), but CPM-labeled gp45 in complex buffer was found to possess freely rotating tryptophan and CPM (*22*), which allows the assumption of κ^2 equal to $^2/_3$ and would yield an error in R_o of less than 10% (*28*). We have found that CPM in V162C/W198F−CPM freely rotates during all stable intermediate states of holoenzyme assembly [the steady-state CPM anisotropy varies between 0.22 and 0.32 (data not shown), consistent with free rotation of CPM]. The largest change in κ^2 would occur if the donor tryptophan is completely rigidified in the intermediate states of holoenzyme assembly, in that case varying between $^1/_3$ and $^4/_3$ (*26*) and yielding a maximal change (an increase or decrease) in R_o of only 4 Å. These individual changes or their accumulation could only partially account for the changes in the W91 to V162C−CPM distances that are reported in Table 4. We therefore feel that the distances shown in Table 4 are reliable representations of the dynamic nature of gp45 during holoenzyme assembly.

The two steps that we have assigned to ATP hydrolysis (steps 3 and 7, Scheme 1) represent only a fraction of the total distance covered by the opening and closing of the gp45 subunit interface. This is unexpected, since it has been proposed that ATP hydrolysis is responsible for powering gp45 opening and closing. We instead suggest based on the information presented in this report that ATP hydrolysis is powering conformational changes in gp44/62. Additional experiments provide support for this suggestion: mixing a nonfluorescent version of gp45 containing 4-fluorotryptophan with gp44/62 and ATP and monitoring changes in tryptophan fluorescence, the gp44/62 tryptophan fluorescence was found to change with an observed rate constant of about 5 s^{-1} (Daniel Sexton, Patrice Soumillion, and Stephen Benkovic, unpublished observations). This observed rate constant is almost identical to the rate constant for ATP hydrolysis in step 3 of Scheme 1. Both gp44 and gp62 contain tryptophans, so it cannot at present be determined which protein is undergoing changes in tryptophan environment concomitant with ATP hydrolysis.

Of considerable interest is the effect of the polymerase on the W91 to V162C−CPM distance in the open subunit interface of gp45. These two proteins form a binary gp45·gp43 complex with a K_d of 48 nM and cause a closure of the open gp45 subunit interface from 40 to 31 Å. This is nearly the same W91 to V162C−CPM distance (30 Å) observed in the holoenzyme complex with DNA ($gp45^K$·DNA·gp43), suggesting that the expenditure of ATP is primarily to position the holoenzyme on DNA so as to ensure processive DNA synthesis. In both cases, gp45 undergoes a substantial conformational reorganization upon binding to gp43, but the contact surface between the two proteins appears to be similar in the two complexes. This closure of the open subunit interface is not observed with the gp43Δ6 mutant that lacks the final six C-terminal amino acids, providing supporting evidence for the importance of the C-terminus of the polymerase in the formation of a productive holoenzyme. The intrusion of the C-terminus of gp43 into the open gp45 subunit interface apparently prevents further closure of this subunit interface to the W91 to V162C−CPM distance of 19 Å representative of a completely closed gp45 subunit interface. The observed rate constant of the second ATP hydrolysis step (step 7, Scheme 1) is very close to that of the reported rate-limiting step for holoenzyme assembly (*5*, *15*). Since we find that this step does not involve opening or closing of gp45, we note that the rate-limiting step for holoenzyme assembly is due to a proposed conformational change in gp44/62, rather than due to a previously proposed conformational change in gp45.

The affinity of the holoenzyme for the DNA can be estimated from the values shown in Table 6. The simulated off rate (step 13, Scheme 1) is about 10 times slower than the rate-limiting step for holoenzyme assembly (step 7, Scheme 1). However, the disassembly of the holoenzyme has been shown to be governed by subunit exchange (*31*), a mechanism that is different than the assembly mechanism shown in Scheme 1. Because the assembly and disassembly mechanisms are not microscopically reversible, a K_d cannot be absolutely assigned. However, the off rate following the same pathway as assembly must be disfavored relative to the subunit-exchange pathway and therefore much slower than the rate of subunit exchange. The simulated off rate can then be treated as an upper limit for the rate of the microscopically revesible pathway, yielding a K_d for the holoenzyme for DNA of probably much lower than 5 nM (the K_d of the gp45−gp43 interaction multiplied by the ratio of the off and on rates from DNA). Our results are consistent with a previous estimate of 20−30 pM based on a different holoenzyme assembly mechanism (*11*, *34*). The K_d of gp43 for DNA has been found to be 70 nM (*36*), so gp45 is serving to increase the affinity of the polymerase for DNA by greater than 10-fold concomitant with a significant increase in processivity.

The results obtained in the present study as well as previous studies (*13*−*15*) on the mechanism of holoenzyme assembly in bacteriophage T4 suggest an assembly mechanism that has differences from that of *E. coli* (*16*−*18*). In *E. coli*, ATP binding is sufficient to form a β clamp·γ complex·DNA complex, with ATP-γ-S an acceptable substitute. We find that ATP-γ-S stalls holoenzyme formation several steps before the analogous gp45·gp44/62·DNA complex. Additionally, experiments in which DNA was added to the

gp45·gp44/62·ATP-γ-S complex did not result in fluorescent changes in the direction associated with productive complex formation. ATP hydrolysis by the γ complex has also been suggested to power γ complex release from the β clamp·DNA complex (*18*). Macroscopically, this is identical with departure of gp44/62 at a step after ATP hydrolysis. However, microscopically it is very different. gp44/62 remains bound to the gp45·DNA complex and chaperones the interaction with gp43 (*5*). We have observed gp44/62 release three steps after the last ATP hydrolysis step. Finally, unlike the stable, unproductive γ complex with ATP-γ-S bound, gp44/62·ATP-γ-S associated with gp45 alone or with both gp45 and DNA readily exchanges ATP-γ-S for ATP within seconds.

Likewise, there are notable similarities between the holoenzyme assembly mechanisms of bacteriophage T4 and *E. coli*. The first is that ATP hydrolysis is not coincident with all of the ring opening and closing events. In the bacteriophage T4 mechanism, step 3 results in both ATP hydrolysis and ring opening, while ring closing in step 5 is not accompanied by ATP hydrolysis but follows in step 7. The first ATP hydrolysis event is not the microscopic reverse of the second: opening of the clamp occurs in the absence of DNA, while its closure occurs in the presence of DNA, so an energy requirement for both processes is not unreasonable. In the *E. coli* mechanism, binding of ATP but not hydrolysis results in ring opening, while ring closing occurs after ATP hydrolysis-coupled departure of the γ complex (*17*). The second is that the formation of the clamp·clamp loader·DNA complexes does not result in complete closing of the clamps. In bacteriophage T4, we find that gp45 will close about an additional 5 Å after the formation of the $gp45^{H}$·gp44/62·DNA complex. Similarly in *E. coli*, the β clamp has a solvent-accessible subunit interface in the β clamp·γ complex·DNA complex (*17*). The L273C position of the β clamp lies at the subunit interface but cannot be labeled with eosin maleimide either free in solution or in a complex with DNA (following γ complex release), suggesting that the β clamp subunit interface is completely closed at the initial and final states of the β clamp·DNA complex formation. The complex between the β clamp and γ complex formed with either ATP or ATP-γ-S and the β clamp·γ complex·DNA complex formed in the presence of ATP-γ-S can all be labeled with eosin maleimide, suggesting that these intermediate states of assembly have an open β clamp subunit interface, analogous to intermediate gp45 assembly states.

In summary, we have demonstrated by stopped-flow FRET that the bacteriophage T4 DNA polymerase holoenzyme is assembled in the multistep process shown in Scheme 1 and diagramed in Figure 7. The gp45 sliding clamp begins open in solution (W91 to V162C−CPM distance of the open gp45 subunit interface of 40 Å) and interacts first with gp44/62. In the presence of ATP, there is a binding event with a simulated K_d of about 0.4 μM followed by fast (100−110 s^{-1}) and then slow (5.5−6.0 s^{-1}) conformational changes. The last change is linked to ATP hydrolysis (since the change is not observed in the absence of nucleotides or in the presence of ADP or ATP-γ-S) and results in gp45 being opened to a W91 to V162C−CPM distance of greater than 45 Å (see Figure 7A). This complex can then either dissociate (0.3−0.4 s^{-1}) or bind to DNA (forward rate constant of 60−80 μM^{-1} s^{-1} and K_d of about 50 nM). Upon binding to DNA, three subsequent conformational changes are observed (175−225, 4.0−4.5, and 0.25−0.30 s^{-1}), with ATP hydrolysis linked to the last change and resulting in gp45 being closed to a W19 to V162C−CPM distance of 35 Å (see Figure 7B). Once again, this complex can either dissociate (0.10−0.15 s^{-1}) or bind to gp43 (forward rate constant of 400−600 μM^{-1} s^{-1} and K_d of about 40 nM). Upon binding to gp43, two subsequent conformational changes are then observed (300−500 and 10−20 s^{-1}), and we propose that the last change is due to dissociation of gp44/62 (see Figure 7C). The final holoenzyme complex has a W91 to V162C−CPM distance of 30 Å, and dissociates with a simulated rate constant of 0.01−0.05 s^{-1}. ATP hydrolysis by gp44/62 accounts for only a fraction of the total changes in the W91 to V162C−CPM distance. We suggest that ATP hydrolysis by gp44/62 is powering conformational changes in gp44/62 that optimizes its interaction with the next component (DNA or gp43) required for loading of the holoenzyme onto DNA, thereby forming a complex capable of processive DNA synthesis.

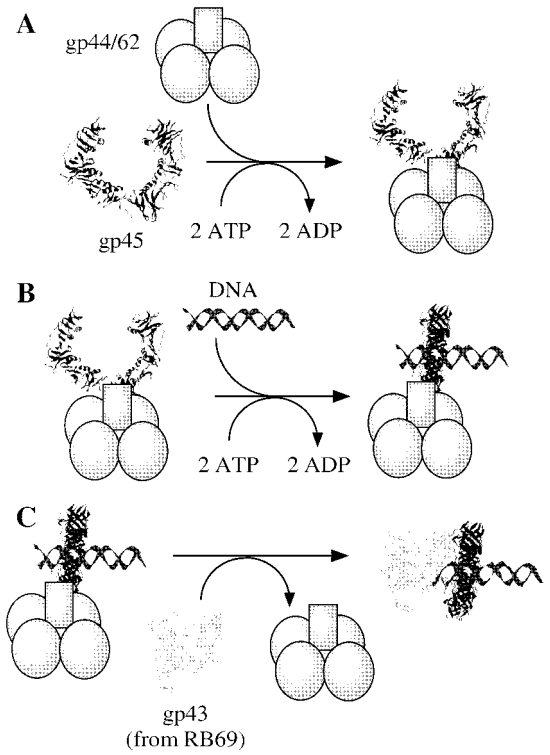

FIGURE 7: Proposed holoenzyme assembly model. (A) Interaction of gp45 and gp44/62 in the presence of ATP. Two molecules of ATP are hydrolyzed in a process that opens the gp45 ring, corresponding to steps 1−3 of Scheme 1. (B) Subsequent interaction of DNA. Two additional molecules of ATP are hydrolyzed in a process that closes the gp45 ring, corresponding to steps 4−7 of Scheme 1. (C) Subsequent interaction of gp43 and dissociation of gp44/62. The final holoenzyme complex is formed in a process that closes the gp45 ring further, corresponding to steps 8−10 of Scheme 1.

ACKNOWLEDGMENT

We thank Ismail Moarefi and John Kuriyan for providing the X-ray crystal structure coordinates of gp45 before publication, as well as Daniel Sexton, Patrice Soumillion, Charles Scott, David Millar, Mark Maroncelli, and Joseph Beechem for helpful discussions.

SUPPORTING INFORMATION AVAILABLE

Four tables containing additional kinetic parameters and one figure containing various multiexponential fits to the data shown in Figure 3. This material is available free of charge via the Internet at http://pubs.acs.org.

NOTE ADDED IN PROOF

M. M. Hingorani et al. [(1999) *EMBO J. 18*, 5131−5144] recently reported a biphasic pre-steady-state burst of ATP hydrolysis by the *E. coli* γ complex in the loading of the β clamp onto DNA, demonstrating a two-step sequential ATP hydrolysis mechanism. These results were obtained using rapid quench methods employing a cold ATP chase, which require tight binding of ATP for success. gp44/62 does not bind ATP tightly, and therefore, a biphasic pre-steady-state burst would not be expected. Sequential hydrolysis of ATP by gp44/62 was alternatively demonstrated by differences in the magnitude of the burst in the presence and absence of DNA.

REFERENCES

1. Kuriyan, J., and O'Donnell, M. (1993) *J. Mol. Biol. 234*, 915−925.
2. Stillman, B. (1994) *Cell 78*, 725−728.
3. Kong, X.-P., Onrust, R., O'Donnell, M., and Kuriyan, J. (1992) *Cell 69*, 425−437.
4. Krishna, T. S. R., Kong, X.-P., Gary, S., Burgers, P. M., and Kuriyan, J. (1994) *Cell 79*, 1233−1243.
5. Kaboord, B. F., and Benkovic, S. J. (1995) *Curr. Biol. 5*, 149−157.
6. McHenry, C. S. (1982) *J. Biol. Chem. 257*, 2657−2663.
7. Studwell-Vaughan, P. S., and O'Donnell, M. (1991) *J. Biol. Chem. 266*, 19833−19841.
8. Podust, V. N., Tiwari, N., Stephan, S., and Fanning, E. (1998) *J. Biol. Chem. 273*, 31992−31999.
9. Wang, C.-C., Yeh, L. S., and Karam, J. D. (1995) *J. Biol. Chem. 270*, 26558−26564.
10. Wang, J., Sattar, A. K. M. A., Wang, C.-C., Karam, J. D., Konigsberg, W. H., and Steitz, T. A. (1997) *Cell 89*, 1087−1099.
11. Berdis, A. J., Soumillion, P., and Benkovic, S. J. (1996) *Proc. Natl. Acad. Sci. U.S.A. 93*, 12822−12827.
12. Alley, S. C., Jones, A. D., Soumillion, P., and Benkovic, S. J. (1999) *J. Biol. Chem. 274*, 24485−24489.
13. Sexton, D. J., Carver, T. E., Berdis, A. J., and Benkovic, S. J. (1996) *J. Biol. Chem. 271*, 28045−28051.
14. Latham, G. J., Pietroni, P., Dong, F., Young, M. C., and von Hippel, P. H. (1996) *J. Mol. Biol. 264*, 426−439.
15. Sexton, D. J., Kaboord, B. F., Berdis, A. J., Carver, T. C., and Benkovic, S. J. (1998) *Biochemistry 37*, 7749−7756.
16. Bloom, L. B., Turner, J., Kelman, Z., Beechem, J. M., O'Donnell, M., and Goodman, M. F. (1996) *J. Biol. Chem. 271*, 30699−30708.
17. Hingorani, M. M., and O'Donnell, M. (1998) *J. Biol. Chem. 273*, 24550−24563.
18. Bertram, J. G., Bloom, L. B., Turner, J., O'Donnell, M., Beechem, J. M., and Goodman, M. F. (1998) *J. Biol. Chem. 273*, 24564−24574.
19. Berdis, A. J., and Benkovic, S. J. (1996) *Biochemistry 35*, 9253−9265.
20. Young, M. C., Weitzel, S. E., and von Hippel, P. H. (1996) *J. Mol. Biol. 264*, 440−452.
21. Turner, J., Hingaroni, M. M., Kelman, Z., and O'Donnell, M. (1999) *EMBO J. 18*, 771−783.
22. Alley, S. C., Shier, V. K., Abel-Santos, E., Sexton, D. J., Soumillion, P., and Benkovic, S. J. (1999) *Biochemistry 38*, 7696−7709.
23. Nossal, N. G. (1979) *J. Biol. Chem. 254*, 6026−6031.
24. Rush, J., Lin, T.-C., Quinones, M., Spicer, E. K., Douglas, I., Williams, K. R., and Konigsberg, W. H. (1989) *J. Biol. Chem. 264*, 10943−10953.
25. Frey, M. W., Nossal, N. G., Capson, T. L., and Benkovic, S. J. (1993) *Proc. Natl. Acad. Sci. U.S.A. 90*, 2579−2583.
26. Selvin, P. R. (1995) *Methods Enzymol. 246*, 300−334.
27. Dunn, B. M., Pham, C., Raney, L., Abayasekara, D., Gillespie, W., and Hsu, A. (1981) *Biochemistry 20*, 7206−7211.
28. Hass, E., Katchalski-Katzir, E., and Steinberg, I. Z. (1978) *Biochemistry 17*, 5064−5070.
29. Cantor, C. R., and Schimmel, P. R. (1980) *Biophysical Chemistry*, Part II, Freeman, San Francisco.
30. Barshop, B. A., Wrenn, R. F., and Frieden, C. (1983) *Anal. Biochem. 130*, 134−145.
31. Soumillion, P., Sexton, D. J., and Benkovic, S. J. (1998) *Biochemistry 37*, 1819−1827.
32. Pietroni, P., Young, M. C., Latham, G. J., and von Hippel, P. H. (1997) *J. Biol. Chem. 272*, 31666−31676.
33. Fu, T.-J., Sanders, G. M., O'Donnell, M., and Geiduschek, E. P. (1996) *EMBO J. 15*, 4414−4422.
34. Kaboord, B. F., and Benkovic, S. J. (1996) *Biochemistry 35*, 1084−1092.
35. van der Meer, B. W., Coker, G., and Chen, S.-Y. S. (1994) *Resonance Energy Transfer Theory and Data*, VCH, New York.
36. Capson, T. L., Peliska, J. A., Kaboord, B. F., Frey, M. W., Lively, C., Dahlberg, M., and Benkovic, S. J. (1992) *Biochemistry 31*, 10984−10994.

BI992377R